Relaxing dispersion pre-distorsion constraints of receiver-based power profile estimators

Louis Tomczyk
LTCI, Télécom Paris,
Institut Polytechnique de Paris
Palaiseau, France
louis.tomczyk@telecom-paris.fr

Élie Awwad
LTCI, Télécom Paris
Institut Polytechnique de Paris
Palaiseau, France

Pétros Ramantanis
Nokia Bell Labs
Nozay, France

Cédric Ware
LTCI, Télécom Paris,
Institut Polytechnique de Paris
Palaiseau, France

***Abstract*—In this work, we offer insights on the advantage of using dispersion pre-distortion (DPD) in correlation-based power profile estimation. We also introduce a method to avoid the use of DPD by replacing it with a receiver-side digital correction of the estimated profile. We assess the accuracy of power anomaly estimation and location of the two methods, namely with or without pre-dipsersion at the transmitter side. Our method demonstrates that both approaches exhibit a similar range of applicability by giving at most relative errors of loss estimation around 20% and location around 2% compared to the ground truth.**

***Index Terms*—digital signal processing, optical network monitoring, power profile estimation, dispersion pre-distorsion**

I. Introduction

Optical telecommunication monitoring strategies have attracted growing attention over the last years as promising solutions to decrease the margins or to increase the availability of the network [1], [2]. Tools have been developed [3]–[8] to identify power losses' locations and/or extract physical parameters of an optical link by estimating the longitudinal power profile along the link using receiver (RX)-based digital signal processing (DSP). On the one hand, [3] noticed that digital Dispersion Pre-Distortions (DPD) of the electrical fields at the transmitter (TX) side has a positive impact on the quality of the detection of anomalies in the link. However, adding DPD is an operation that we would like to avoid since it is known to increase NonLinear Interference (NLI) distortions [10]–[12] and may lead to a reduction of the available margins or even an outage. We first numerically investigate on how DPD affects the profile estimator; then we suggest an approach to link the DPD and NLI in order to understand why DPD impacts the final output of the estimator. Later, we describe a method to avoid DPD by applying instead a correction to the RX-side estimated profile. Finally, we assess the accuracy of detecting and evaluating a power anomaly inserted at several locations in a span when TX-side DPD or RX-side profile correction is used. We conclude that both methods can provide similar acccuracy for loss estimation and location within the same range of applicability (loss values lower than 6 dB).

II. Correlation-based profile estimator and simulation setup

Throughout this work, we rely on the algorithm suggested in [3] that gives a Pearson's correlation based profile $z \mapsto R(z)$ between the complex amplitudes of two fields as a function of the distance z. The first field is reconstructed from decided symbols (or known symbols at the RX-side) and the second field is retrieved after polarization separation and undergoes a partial remediation of the nonlinear phase. We refer the reader to [3] for additional details on the algorithm. Unless otherwise specified, the simulation setup is the following. We focused on a point-to-point optical fibre communication link made of N_{spans} of identical Standard Single Mode Fibres (SSMF) of length $L_{\mathrm{span}} = 100$ km, with an attenuation coefficient $\alpha_{\mathrm{dB}} = 0.22$ dB/km and a nonlinear parameter $\gamma = 1.31\ (\mathrm{W}\cdot\mathrm{km})^{-1}$ at the wavelength of 1550 nm. The SSMF has a chromatic dispersion coefficient $D_{\mathrm{CD}} = 16.7$ ps/nm/km and slope $S_{\mathrm{CD}} = 0.058$ ps/nm^2/km at the same specified wavelength. Polarization Mode Dispersion (PMD) is taken into account with $D_{\mathrm{PMD}} = 0.04$ ps/$\sqrt{\mathrm{km}}$ as well as the polarization coupling. The transmitted data (800 sequences of $N_{\mathrm{symb}} = 2^{14}$ symbols for each obtained profile) are sent at a symbol rate $R_{\mathrm{s}} = 28$ GBd and were carried by a single Polarization-Division-Multiplexed (PDM) channel. The modulation format is Quadrature Phase Shift Keying (QPSK) and the signal was shaped using a Root Raised-Cosine (RRC) filter with a roll-off factor $\beta_{\mathrm{roll}} = 0.01$. Also, at the transmitter side, we digitally add a desired value of accumulated dispersion pd expressed in ps/nm. The power into the link is $P_{\mathrm{in,dBm}} = 4$ dBm. The sampling frequency is set with a Shannon coefficient of 8. The propagation is simulated using the Split-Step Fourier Method (SSFM) with a resolution of 1 km. Eventually the noiseless EDFAs are set to perfectly compensate the loss in a span (gain $G_{\mathrm{dB}} = 22$ dB). Fig. 1 shows the profiles R obtained with the algorithm for $N_{\mathrm{spans}} = 5$ without DPD (black solid line), and $R^{(5100)}$ with $\mathrm{pd} = 5100$ ps/nm (pink solid line). We also show the envelope of the profiles (dashed lines and markers) on the same figure. obtained my estimating the extrema locations and joining them together.

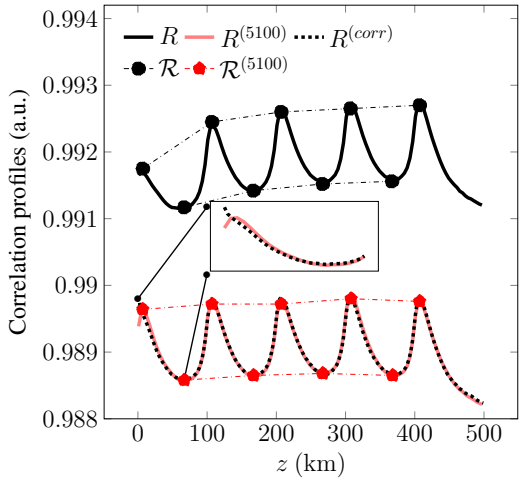

Fig. 1. Example of profiles given by the estimator R, $R^{(5100)}$, their envelope $\mathcal{R}, \mathcal{R}^{(5100)}$ as well as the corrected profile $R^{(corr)}$.

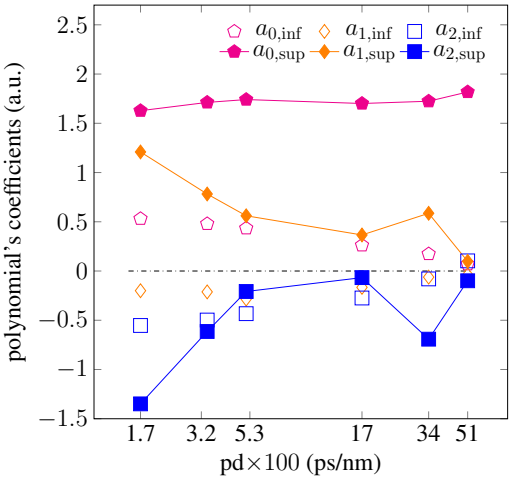

Fig. 2. Evolution of polynomial coefficients with pre-dispersion displayed on a logarithmic scale.

It is clear that the envelope of the original profile $\mathcal{R}$ is more curved than the pre-dispersed one, $\mathcal{R}^{(5100)}$. This means that, if no DPD is used, the monitored longitudinal power profile contains an artificial distortion, especially at the beginning of the transmission link, a distortion which is not present when DPD is used. Only five spans are shown here in order to easily distinguish the different curves. However, we can already spot the curved envelope of the profile in black especially for the first span. The parabolic shape of the envelope is much more obvious for a link having a larger number of spans. The inset in Fig. 1 shows a zoomed view of the first span to emphasize on the shape of the estimated profile for the first few kilometers. The corrected profile $R^{(corr)}$ will be discussed in section IV. We quantify the flatness of the envelope by fitting the local extrema of the scaled profile with mean zero and unit standard deviation $\widetilde{R} = [R - \mathbb{E}(R)]/\sigma(R)$ with a second order polynomial whose coefficients are: $(a_{\text{k,inf/sup}})_{\text{k}\in\{0,1,2\}}$: $\tilde{\mathcal{R}}_{\text{inf/sup}}(z) = a_{0,\text{inf/sup}} + a_{1,\text{inf/sup}} z + a_{2,\text{inf/sup}} z^2$. $\mathbb{E}(\bullet)$ and $\sigma(\bullet)$ corresponds respectively to the empiric average and standard deviation of $\bullet$, and the index inf/sup corresponds to the inferior/superior part of the envelope respectively. The evolution of the coefficients with an increasing pd are shown in Fig. 2. The coefficient $a_{0,\text{inf/sup}}$ can be seen as the mean value of whether the inferior/superior part of $\widetilde{R}$ and $a_{1,2/\text{inf,sup}}$ as its curvature. We notice that increasing pd reduces the curvature and makes the mean values converge to constants. From $\text{pd} = 170$ ps/nm to $\text{pd} = 5100$ ps/nm, the coefficients $a_{1,2/\text{inf,sup}}$ were divided by more than five at this symbol rate. This fit quantifies and shows the advantage to use DPD for a better estimation of the true power profile.

III. Impact of pre-dispersion

In the previous section, we quantified how much the use of DPD flattens the profile. In order to understand why it is a key point, we study the Deviation-to-Average Power Ratio of the received optical signal, DAPR, defined as: $\text{DAPR} = \sigma(P)/\mathbb{E}(P)$ where P is the instantaneous power. Fig. 3 shows the evolution of the DAPR with pd for different symbol rates after propagation in only one span. The accumulated chromatic dispersion (or digital pre-dispersion pd) mixes more and more symbols up to the point where mixing more symbols no longer increases the DAPR significantly as all curves reach a saturation regime. In the meanwhile, a signal reaches the same DAPR value with less pd for higher symbol rates.

This observation can be linked to the excitation of the non-linear effects using NLI models. It is common to quantify NLI by writing its variance as $\sigma^2_{\text{NLI}}(n) = A_{\text{NLI}}(n) P^3_{\text{in}}$ [9], [11], where P_{in} is the average power into the link (in watts), and $n \in [\![1, N_{\text{spans}}]\!]$ the span number. In [9], the authors showed that the NLI coefficient A_{NLI} can be itself written as $A_{\text{NLI}} = a_{\text{NLI}} \cdot N_{\text{span}}^{1+\varepsilon}$ where a_{NLI} is the NLI coefficient after one span and ε takes depends on the system parameters. In our work, we compute the A_{NLI} following the method detailed in [11] with the sole difference that we use a minimum distance decoder to estimate the phase of each symbol instead of the data-aided approach. Fig. 4 shows the evolution of a_{NLI} with the DPD (after propagation over a single span $N_{\text{span}} = 1$). We observe a sigmoidal evolution (tanh function) of the NLI similar to that of DAPR. The behavior is expected at low dispersion values, such as for Dispersion Shifted Fibres (DSF), in a single channel case. Indeed, dispersion transforms the shape of the impulse by spreading it over time. No dispersion implies that the amplitude remains unaltered and the DAPR retains the same value. However, non-zero dispersion results in a positive offset of the lower plateau in the curve due to amplitude distortions. Our simulations demonstrate that neither the type of fibre (SMF, Large Effective Area Fibre [10], DSF, Non-Zero DSF), the launched power $(0, 2, 4$ dBm), the span length $(10, 25, 50, 75, 100$ km), the number of spans (ranging from 1 to 10), nor the used modulation scheme (QPSK, 16/32/64-Quadrature Amplitude Modulation), affect the overall sigmoidal shape of the DAPR at both the trans-

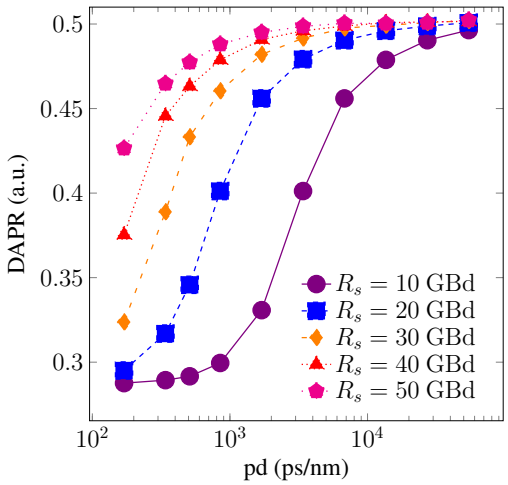

Fig. 3. Impact of the DPD on the Deviation-to-Average Power ratio after a single span.

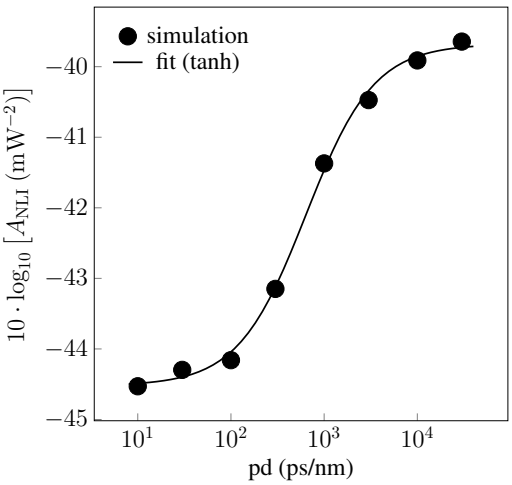

Fig. 4. Impact of the DPD on the NLI coefficient for one span.

mitter and receiver ends (only the plateau levels and inflection point location are affected). Figures are not shown here for lack of space.

IV. Profile Correction

In this section, we suggest a method to avoid the use of DPD by RX-side compensation of the profile, that we will refer to as the "correction" method. We can explain the curve-shaped envelope in non pre-dispersed profiles using the evolution of the NLI coefficient. Indeed the DPD helps to flatten the correlation profile by increasing the nonlinear distortions in the first spans. This is due to the fact that the algorithm evaluates the similarity between the transmitted field and the partially non-linear equalized received field. However, its impact is less important for the last spans because the deviations of the instantaneous signal power have already reached their saturation regime. Thus, we can see DPD as a way to ensure a minimum level of A_{NLI} all along the link that gives the flattened profile. Keeping this observation in mind, we propose an alternative method of flattening the estimated profile. First, we focus on the evolution of A_{NLI} and we aim to find a function that enables to achieve in each point of the link the same NLI variance as the one at the end of the link $A_{\mathrm{NLI}}(N_{\mathrm{spans}})$. This leads to finding a function $z \mapsto F(z)$ that verifies Eq (1) below. Thus, by taking the derivative of the equation with respect to n, it yields the well-known exponential solution.

$$\forall n \in [\![1, N_{\mathrm{spans}}]\!] \quad A_{\mathrm{NLI}}(n)F(n) = A_{\mathrm{NLI}}(N_{\mathrm{spans}}) \tag{1}$$

$$\implies \quad F(n) = (N_{\mathrm{spans}}/n)^{1+\varepsilon} \tag{2}$$

The solution can be rewritten by suggesting a continuous version with the distance z if we replace $n = \lfloor z/L_{\mathrm{span}} \rfloor$ and $N_{\mathrm{span}}L_{\mathrm{span}} = L_{\mathrm{link}}$ leading to $F(z) = (L_{\mathrm{link}}/z)^{1+\varepsilon}$.

As we want to process the correlation profiles at the RX-side so that they become similar to the ones obtained with DPD at TX-side (meaning with a maximum amount of A_{NLI} in the first spans), we apply a "Correction Function" similar to the one proposed to compensate the A_{NLI} in the link: $F_{\mathrm{C}}(z) = z^{-A_{\mathrm{F_C}}}$ with $A_{\mathrm{F_C}} > 0$, such as $R^{(\mathrm{corr})}(z) = F_{\mathrm{C}}(z) \cdot R(z)$. The coefficient $A_{\mathrm{F_C}}$ can be empirically calculated knowing the symbol rate, and can be used afterwards. Its value is obtained by simulating the profile with different symbol rates with two extreme values of pd. We get the first profile R with $\mathrm{pd} = 0$ ps/nm and we get the second one, $R^{(pd)}$, with the value of pd required to reach the saturating regime of the DAPR (see Fig. 3). We pursue by computing the ratio $R^{(pd)}/R$ and by fitting the latter to get the correction function F_{C}. An example of the use of this correction is shown in Fig. 1 with the black dotted line. The corrected profile overlaps with the pre-dispersed one by construction of the correction function which explains the offset with respect to the original profile (without DPD). We noticed that $A_{\mathrm{F_C}}$ is independent of the number of spans and the number of transmitted symbols, not shown here for lack of space. Finally, we report the values of the fit coefficient $A_{\mathrm{F_C}}$ for different symbol rates on Fig. 5. As highlighted in the previous section, we expect that the symbol rate will have a major impact which is translated in a power dependence of $A_{\mathrm{F_C}}$ with respect to it. Indeed, an asymptotic study of the dependence of ε given by Eq. (40) in [9] on the transmission parameters reveals, using the group velocity dispersion, β_2, that:

$$\varepsilon \underset{R_{\mathrm{s}} \to +\infty}{\sim} \frac{18}{5\pi^2 \cdot |\beta_2| L_{\mathrm{span}} \cdot [(1+\beta_{\mathrm{roll}}) \cdot R_{\mathrm{s}}]^2} \tag{3}$$

In Fig. 5, the formula used for $A_{\mathrm{F_C}}$ is proportional to $R_{\mathrm{s}}^{-1.79}$. We can notice that the exponent is close (1.79 instead of 2 in Eq. (3)). In addition, the correction is less and less needed as we increase the symbol rate.

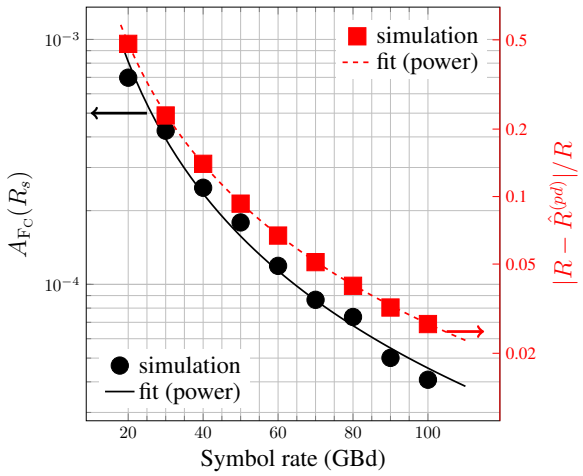

Fig. 5. Evolution of the coefficient $A_{\mathrm{F_C}}$ in the correction function F_{C} (black) and of the relative error after correction (red) with respect to the symbol rate.

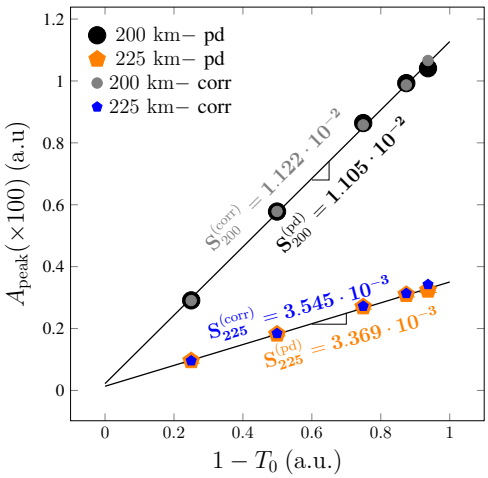

Fig. 6. Peak values of the anomaly indicator after use of DPD or with the correction method.

This was expected as, at higher data rates, more symbols interfere creating a higher DAPR and triggering, sooner in the link, higher non-linear distortions. This is shown by the the red curve that gives the evolution of the relative error $|R - R^{(corr)}|/R$ with the symbol rate, which quickly tends to zero. Moreover, the relative error $|R^{(corr)} - R^{(pd)}|/R^{(pd)}$ is also quite low (< 0.1 %), which confirms the efficiency of the correction method to flatten the profile.

V. Impact of the Correction on the Loss Estimations Accuracy

A. Anomalies estimation setup

The goal is to get both locations and amplitude estimations $(\hat{z}_{\mathrm{loss}}, \hat{\ell}_{\mathrm{dB}})$ of inserted losses in a span. Here, the setup is the same as described in section II with the following modifications in order to match with the setup in [7] with the only difference that the propagation is simulated with a single-polarisation, single-channel. The link is made of three identical 100 km SSMF spans with an attenuation of $\alpha_{\mathrm{dB}} = 0.206$ dB/km and with amplifiers having a noise figure of 5 dB. Each profile is obtained with 3000 sequences of 2^{10} symbols sent at a symbol rate of $R_{\mathrm{s}} = 32$ GBd with an input power of $P_{\mathrm{in,dBm}} = 5$ dBm. We simulate different loss values ℓ_{dB} (in dB) and different locations z_{loss} (in km). The loss in linear scale is noted $1 - T_0$ where $T_0 = 10^{-\ell_{\mathrm{dB}}/10}$ such as ideally $R_{\mathrm{mon}}(z_{\mathrm{loss}}) = T_0 \cdot R_{\mathrm{ref}}(z_{\mathrm{loss}})$ where "mon" stands for "monitored" profile and "ref" stands for "reference" profile. The estimation method is the same as described in [7] and starts with the computation of a calibration coefficient C that links the correlation profile R with a power profile $\mathcal{P}$ such that: $R = C \cdot \mathcal{P} + \theta$ where θ is an offset. Here we will note $\bullet^{(\mathrm{pd/corr})}$ the quantity $\bullet$ obtained after performing DPD (pd = 3000 ps/nm) or after performing the correction respectively. Then, we compute the "Anomaly Indicator" AI defined as: $\mathrm{AI}^{(\mathrm{pd/corr})} = R_{\mathrm{ref}}^{(\mathrm{pd/corr})} - R_{\mathrm{mon}}^{(\mathrm{pd/corr})}$.

$$A_{\mathrm{peak}}^{(\mathrm{pd/corr})} = \underbrace{\frac{C^{(\mathrm{pd/corr})}}{10^{\alpha_{\mathrm{dB}} \cdot \Delta z^{(\mathrm{k})}/10}} \cdot P_{\mathrm{ref}}}_{S_{\Delta z^{(\mathrm{k})}}^{(\mathrm{pd/corr})}} \cdot (1 - T_0) \tag{4}$$

We noted $R_{\mathrm{ref/loss}}^{(\mathrm{pd/corr})}$ the reference/monitored profile after having inserted a loss computed with DPD or after correction respectively. The peak of the AI is linked to the loss by Eq. (4) where we use the same notations as in [7]. Thus, $\Delta z^{(\mathrm{k})} = z_{\mathrm{loss}} - z^{(\mathrm{k})}$ is the distance of a loss from the k-th span, and P_{ref} the power at the output of the amplifier used for the calibration. In Eq. (4), we can see that the loss estimation will vary with C, A_{peak} and $\Delta z^{(\mathrm{k})}$. In order to fully characterise the correction method in terms of accuracy, we will evaluate the loss estimations by studying the impact of the variations of A_{peak} and $\Delta z^{(\mathrm{k})}$ separately, then with both at the same time. We further assume that the calibration step, consisting in finding the term $C \cdot P_{\mathrm{ref}}$, is done once and for all. Finally, all the data points are the empirical mean of twenty realisations and the 3σ-error bars are plotted.

B. Results

1) Calibration: Here, we first determine the impact of the correction on the calibration step meaning that $\delta \Delta z^{(\mathrm{k})} = 0$. In Fig. 6, we plot the peak amplitude of the anomaly indicator with respect to the inserted loss. The calibration has been performed with a loss of 3 dB. The error bars here are not visible, compared to [7], as their order of magnitude is 10^{-5}. This can be explained by the fact that in this paper the simulations do not take into account the multiple sources of noise that can be found in experiments (transceivers, uncertainties, etc.). Then, we added four linear regressions, one for each method and for each distance. For a given distance, the regressions for the two methods cannot be distinguished as they overlap. Finally, the slopes are given when using DPD or the correction method.

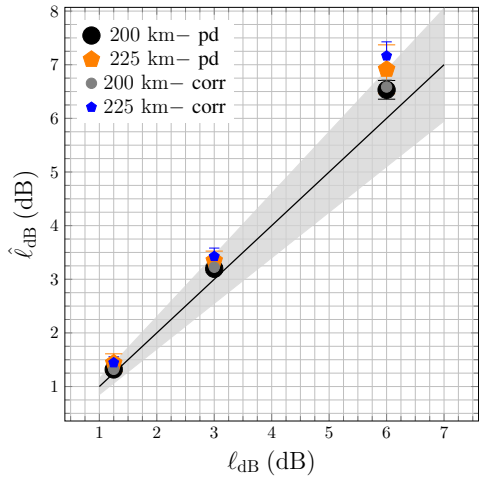

Fig. 7. Estimated loss values $\hat{\ell}_{\mathrm{dB}}$ when loss location are known: $\delta\Delta z^{(\mathrm{k})} = 0$. The shaded area corresponds to an error of $\pm 15\%$.

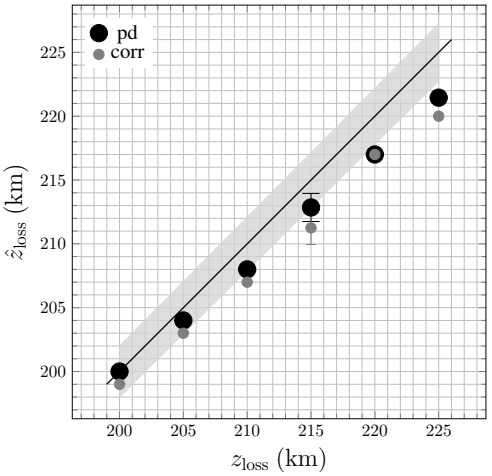

Fig. 8. Estimated loss location values $\hat{z}_{\mathrm{loss}}$ function of the true location z_{loss}. The shaded area corresponds to an error of $\pm 1\%$.

We can first notice that the peak values for both methods are quite well overlapping and the slope values are also similar, meaning that the correction method does not affect significantly the peak amplitude. Secondly, if we perform the ratio of the slopes at 200 km with the ones at 225 km we respectively get for the DPD and correction method 3.28 and 3.17 instead of $10^{0.206 \cdot 25/10} \approx 3.27$. This represents an error of around 3% for the correction method compared to the use of DPD. Finally, the peak values differ by a factor 20 compared to [7] for the following reasons: a factor two comes from the single/dual polarisation hypothesis. While the factor ten comes from the fact that in our simulations, the received field is not normalised and a power of 5 dBm = 3.16 mW leads to a factor ten when the correlation is computed.

2) Peak values induced errors: Now we study how the inaccuracies on the peak amplitude affect the estimation of the loss by assuming $(\delta\Delta z^{(\mathrm{k})}, \delta C) = (0, 0)$. In Fig. 7, we plot the estimated loss as a function of the inserted loss of $\{1.25, 3, 6\}$ dB even though computations have also been done for higher losses $\{9, 12\}$ dB. The solid line corresponds to the identity ($\hat{\ell}_{\mathrm{dB}} = \ell_{\mathrm{dB}}$). The shaded area corresponds to an error of $\pm 15\%$. Similarly to the peak evolution, we plotted the estimated loss with DPD or with the correction for the two distances. We can firstly notice that when the loss is located at the amplifier, errors are always included within the 15% limit. Secondly, except for the correction at 225 km, the errors are still in those boundaries. However, for the correction case beyond 6 dB, errors quickly increase (from 0.7 to $>$ 12 dB). These points are not shown in order to ease the reading for low inserted loss values. However, distinguishing higher loss values is irrelevant as beyond 6 dB is an extreme case of anomaly. To understand why the correction method gives such errors, we need to come back to the AI. The peak in the AI can be expressed after applying the correction method using Eq. (5). This correction function induces a slight change on A_{peak} that will propagate up to the estimated loss.

$$A_{\mathrm{peak}}^{(\mathrm{corr})} = \max_{z} \Big([R_{\mathrm{ref}}(z) - R_{\mathrm{mon}}(z)] \cdot F_{\mathrm{C}}(z) \Big) \tag{5}$$

The excess loss induced by a change $\delta\bullet$ on $\bullet$, written $\delta\hat{\ell}_{\mathrm{dB}}^{\bullet} = \hat{\ell}_{\mathrm{dB}}(\bullet + \delta\bullet) - \hat{\ell}_{\mathrm{dB}}(\bullet)$, is given by Eq. (6).

$$\delta\hat{\ell}_{\mathrm{dB}}^{A_{\mathrm{peak}}} = -10\log_{10}\left(1 - \left[10^{\ell_{\mathrm{dB}}/10} - 1\right] \cdot \frac{\delta A_{\mathrm{peak}}}{A_{\mathrm{peak}}}\right) \tag{6}$$

For instance, a deviation $\delta A_{\mathrm{peak}}/A_{\mathrm{peak}} \approx 6\%$ produces an error of only 0.33 dB for $\ell_{\mathrm{dB}} = 1.25$ dB at a given distance. However, this same error gives an error of more than 12 dB for $\ell_{\mathrm{dB}} = 12$ dB at the same distance. It is noteworthy to emphasize that Eq. (6) is not limited to the correction method alone, but also holds true for DPD.

3) Locations induced errors: As pointed out in [7], accurate location information is critical for minimising errors. Therefore, we investigate the impact of variations in location, $\delta\Delta z^{(\mathrm{k})}$, on the accuracy of loss estimation. We insert a loss of 3 dB at different locations $z_{\mathrm{loss}} \in \{200, 205, 210, 215, 220, 225\}$ km. Unlike [3] and [7], we estimate the location of losses based on the maximum of the AI: $\hat{z}_{\mathrm{loss}} = \underset{z}{\mathrm{argmax}}[\mathrm{AI}(z)]$. The estimated loss locations as a function of the true loss location are plotted in Fig. 8. The shaded area corresponds to a $\pm 1\%$ error case this time. The solid line represents the identity. Both algorithms tend to underestimate the loss location, and the error bars are often not visible due to the small step resolution of 1 km used in both the SSFM and the profile estimator, which is insufficient to observe fluctuations. Additionally, for both methods, the error in location appears to increase with distance, as noticed experimentally by the authors in [7]. On average, the error in location estimation is approximately 2.0 km for the DPD method and 2.8 km for the correction method, representing a

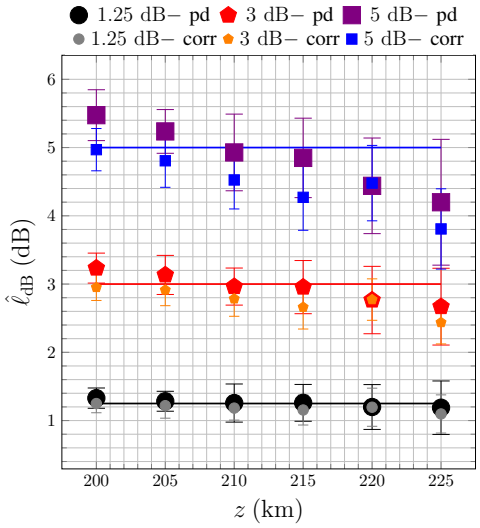

Fig. 9. Estimated loss values $\hat{\ell}_{\mathrm{dB}}$ function of the true location z_{loss} with unknown loss location $\Delta z^{(\mathrm{k})} \neq 0$.

40% difference compared to the DPD method. We can derive a formula, Eq. (7), to quantify the error on the estimation of the loss resulting from location inaccuracies. For instance, a 3 dB inserted loss results in estimation errors of 0.22 dB for $\Delta z^{(\mathrm{k})} = 1$ km and 1.4 dB for $\Delta z^{(\mathrm{k})} = 5$ km.

$$\delta\hat{\ell}_{\mathrm{dB}}^{\Delta z^{(\mathrm{k})}} = \ell_{\mathrm{dB}} - 10\log_{10}\left(1 - \left[1 - 10^{-\ell_{\mathrm{dB}}/10}\right] \cdot 10^{\alpha_{\mathrm{dB}}\delta\Delta z^{(\mathrm{k})}/10}\right) \quad (7)$$

4) Anomaly location and estimation: Finally, we take both variations (location and loss value) into account by locating the amplifier location using the local maxima of the power profile before locating the loss in a given span. The estimated location of the amplifier is $z^{(2)} = 206$ km. We inserted three different losses $\ell_{\mathrm{dB}} = \{1.25, 3, 5\}$ dB at the same locations as previously. Fig. 9 shows the resulting estimations of the loss for both methods. Compared to Fig. 7, both approaches exhibit similar trends of underestimating the loss value, as in [7], which can be explained by the understimation of the loss location as seen in Fig. 8. This fact confirms the claim that loss location estimation is a key point. Additionally, the correction in average always underestimate the loss compared to the DPD of respectively 0.1, 0.2 and 0.4 dB, across different locations relpresenting relative errors around 20% for the evaluation of the loss compared to the ground truth.

VI. Conclusion

In this study, we investigated the effectiveness of using pre-dispersion to flatten power profiles, which resulted in a reduction in power profile variations by more than fivefold. Additionally, we observed that pre-dispersion stimulates nonlinear effects and increases the DAPR of the power, leading to saturation in the regime of A_{NLI}. Based on these observations, we proposed a DSP-based method on the RX-side to recover the power profile that would have been obtained with pre-dispersion. Our method demonstrated high accuracy in flattening the profile with very low relative errors. We also evaluated the accuracy of our method in estimating both the location and loss value and we derived formulas to assess the impact of parameter variations. Our method was effective up to a loss value of 5 dB, beyond which using both DPD and the corrections resulted in diverging loss estimations as predicted by our derivations. Moreover, we also observed the crucial role of loss location estimation for accurate loss evaluation as it results in inversing the trend from overestimation for known location to underestimation for unknown ones. In average, simulations have showed relative errors compared to the ground truth around 20% and 2% respectively for the loss evaluation and location. Future work will investigate the need for digital pre-distortion in other power profile estimation methods.

VII. Acknowledgement

This work has received funding from BPI France (grant 0168463/00) within the CELTIC-NEXT European project AI-NET Antillas.

References

[1] Y. Pointurier, *Design of low-margin optical networks*, Proc. Optical Fiber Conference (OFC), 2016
[2] K. Christodoulopoulos et. al, *Toward efficient, reliable, and autonomous optical networks: the ORCHESTRA solution*, IEEE J. Opt. Commun. Netw., Sept. 2019, Vol 11, No. 9
[3] T. Tanimura et. al, *Fiber-longitudinal anomaly position identification over multi-span transmission link out of receiver-end signals.*, J. Light. Tech, May. 2020, Vol 38, No. 9
[4] T. Sasai et. al, *Simultaneous detection of anomaly points and fiber types in multi-span transmission links only by receiver-side digital signal processing.*, Proc. Optical Fiber Conference (OFC), 2020
[5] T. Sasai et. al, *Closed-form Expressions for Fiber-Nonlinearity-Based Longitudinal Power Profile Estimation Methods*,Proc. European Conference on Optical Communication (ECOC), 2022
[6] S. Gleb et. al, *Fiber link anomaly detection and estimation based on signal nonlinearity.*, Proc. European Conference on Optical Communication (ECOC), 021
[7] A. May et. al, *Receiver-based experimental estimation of power losses in optical networks.*, Phot. Tech. Lett., Nov. 2021, Vol. 33, No. 22
[8] A. May et. al, *Receiver-Based Localization and Estimation of Polarization Dependent Loss*, Proc. OptroElectronics and Communications Conference (OECC), 2022
[9] P. Poggiolini et. al, *The GN-Model of Fiber Non-Linear Propagation and its Applications.*, J. Light. Tech. Vol 32, No 4, Feb. 2014
[10] E. Seve et. al, *Semi-analytical model for the performance estimation of 100Gb/s PDM-QPSK optical transmission systems without inline dispersion compensation and mixed fiber types.*, Proc. European Conference on Optical Communication (ECOC), 2013
[11] N. Rossi et. al, *Nonlinear Interference noise statistics in unmanaged coherent networks with channels propagating over different lightpaths.*, Proc. European Conference on Optical Communication (ECOC), 2014
[12] R. Dar et. al, *Properties of nonlinear noise in long, dispersion-uncompensated fibre links.*, Opt. Express, Nov. 2013, Vol 21, No. 22